A Novel Predictive Fuzzy Logic-Based Energy Management System for Grid-Connected and Off-Grid Operation of Residential Smart Microgrids

Jafari, M.; Malekjamshidi, Z.; Zhu, J.; Khooban, M.

Published in:
IEEE Journal of Emerging and Selected Topics in Power Electronics

DOI (link to publication from Publisher):
10.1109/JESTPE.2018.2882509

Publication date:
2020

Document Version
Accepted author manuscript, peer reviewed version

A Novel Predictive Fuzzy Logic-Based Energy Management System for Grid-connected and Off-grid Operation of Residential Smart Micro-grids

Mohammad Jafari, *Member, IEEE,* Zahra Malekjamshidi, *Student Member, IEEE*, Jianguo Zhu, *Senior Member, IEEE, and* Mohammad-Hassan Khooban, *Senior Member, IEEE*

***Abstract*—**In this paper, a novel energy management system with two operating horizons is proposed for a residential micro-grid application. The micro-grid utilises the energies of a photovoltaic (PV), a fuel cell and a battery bank to supply the local loads through a combination of electric and magnetic buses. The proposed micro-grid operates in a large number of grid-connected and off-grid operation modes. The energy management system includes a long-term data prediction unit based on a 2D dynamic programming and a short-term fuzzy controller. The long-term prediction unit is designed to determine the appropriate variation range of the battery state of charge and fuel cell state of hydrogen. The efficiency performance of the micro-grid components, predicted energy generation and demand, energy cost and the system constraints are taken into account. The resultant data then is sent to the short-term fuzzy controller which determines the operation mode of the micro-grid based on the real-time condition of the micro-grid elements. A prototype of the proposed micro-grid including the energy management system is developed, and experimental tests are conducted for three different energy management scenarios. The proposed management technique is validated through energy distribution and cost analysis.

***Index Terms*—**Energy management, fuzzy logic control, residential micro-grid, predictive control, renewable energy system

I. INTRODUCTION

DISTRIBUTED renewable generation systems are known as the feasible solution for environmental pollution, increasing electricity demand and reduction of energy transmission losses. The total share of renewable energy must rise from around 15% of the total primary energy supply in 2015 to around two-thirds by 2050, to meet climate targets set out in the Paris agreement [1]. Furthermore, the share of renewable energy systems (RESs) in the building sector should be increased from 36 % in 2015 to 77 % [1]. In Australia, the cumulative number of installed rooftop solar systems reached to 1.8 million installations by the end of 2017 [2]. The concept of residential smart micro- grids emerged with the increasing influence of the household grid-connected RESs on stability and power quality of the distribution networks [5]. In this regard, various energy management techniques are proposed in the literature to match the energy generation and consumption inside the micro-grid optimally and minimize the customer and grid interventions [6], [7]. In the simplest form, the energy control boxes have been used to manage the energy consumption of household and reduce the energy bills by shifting loads to the off-peak hours [7]. This also benefits the main grid by reducing the peak energy demand, power loss on transmission lines and redundant power stations [8]. Therefore, new provisions related to the grid-connected RESs, encourage the consumers to change from passive energy users to the active generators and contribute to supplying energy and network power quality [9]. As a result, intelligent energy management systems, multi-operation mode converters, smart household appliances and local communication networks are recommended in the new standards [10]. Furthermore, the micro-grids are required to communicate with the regional smart grid control centre by using a higher level communication networks (cellular networks and 4G technologies such as WiMAX) to adapt their operation with the requirements [11]. In this regard, a large number of research focusing on different micro-grid topologies and control techniques, optimal energy management methods, various scenarios and objectives have been presented in the literature [12]-[14]. In the case of micro-grid topologies, the most common structure utilizes multiple converters to link the renewable sources to a common dc or ac electrical bus [15], [16]. However, this structure leads to complex control methods and frequency and voltage stability techniques [17]. A second option in the case of small-scale applications such as residential micro-grids is using a magnetic bus (multi-winding transformer) to integrate the renewable energies in the form of magnetic flux [18],[19]. This reduces the voltage conversion stages which results in the smaller size, lower cost, higher conversion efficiency, and better safety and reliability due to the isolation of the micro-grid components [20]. Furthermore, a simpler control technique is required as there is no voltage and frequency instabilities [21]. However, this method is not suitable for a large number of the micro-grid elements due to the complexity of multi-winding transformer design [18]. In this case, a combination of electrical and magnetic buses is recommended as presented in this paper. On the other hand, the energy management methods inside the micro-grids can be classified as rule-based and optimization based methods [22]. The rule-based techniques use the real-time value of the micro-grid

Manuscript received August 16, 2018; revised October 15, 2018; accepted November 8, 2018.

M. Jafari and Z. Malekjamshidi are with the School of Electrical and Data Engineering, University of Technology Sydney, NSW, Australia.
e-mail:(mohammad.jafari@uts.edu.au; z.malekjamshidi@uts.edu.au)

Jianguo Zhu is with the School of Electrical and Information Engineering, The University of Sydney, NSW, Australia.
(e-mail: Jianguo.zhu@sydney.edu.au)

M.H.Khooban is with the Department of Energy Technology, Aalborg University, 9220 Aalborg East, Denmark. (e-mail: kho@ et.aau.dk).

parameters to manage the power flow in the system and are categorized as deterministic [23], and fuzzy rule-based methods [24]. Among the rule-based real-time energy management techniques, Fuzzy controllers have attracted interest.

In contrast to the deterministic rule-based control methods, fuzzy controllers are independent of intrinsic nonlinearities of the micro-grid components and therefore, do not need complex mathematical modelling [25]. This leads to a comprehensive energy management system (EMS) based on the simple linguistic rules and reduces the control complexity in the case of a micro-grid with a large number of operation modes (such as the micro-grid proposed in this paper). In [26], a fuzzy logic supervisory control is designed to manage the power flow in an electric vehicle drive train containing a fuel cell as power source and batteries and super capacitors as storage devices. Similar applications are reported in [22] and [27]. In the case of micro-grid applications, fuzzy logic based energy management systems (FLBEMSs) have been proposed for various objectives. Diego et al. proposed a FLBEMS for a residential micro-grid to minimize the grid power fluctuations taking into account the battery SOC limits. However, proper selection of the system operation modes is not included in the control rules [15]. A multi-agent FLBEMS is designed to optimally control the battery system in a residential micro-grid in [28]. An automatic EMS combining the fuzzy controller and neural networks for energy efficient home is presented in [29]. However, none of these systems deals with a real-time energy cost profile as this paper is doing.

On the other hand, to optimize the energy management operation, different techniques based on the fuzzy logic [30],[31], genetic algorithms [32], artificial neural networks [33], particle swarm optimization [34] dynamic programming [35]-[37], linear programming [38], mixed integer linear programming [39] and quadratic programming [40] are presented in the literature. The quadratic programming needs relaxation techniques using Lagrangian multipliers [39]. In [30], three approaches based on fuzzy logic, mixed integer linear programming (MILP) and MILP with continuous relaxation techniques have been studied to perform the rolling optimization of a home EMS. It is shown that the fuzzy logic based method can provide better performance in terms of the computational time, cost, optimization performance and independence on the forecasted data. A weighted improved DP based technique along with a real-time PID controller is proposed in [35] to control a fuel cell hybrid vehicle optimally. A DP based optimization technique is proposed in [37] to perform the peak shaving of a grid-connected PV/battery system with minimum cost and presented satisfactory results compared to a simple rule-based control. However, the proposed systems are much simpler in the system topology and contain less number of variables, operation conditions (off-grid and grid connected) and optimization effective parameters compared to what is proposed in this paper. Therefore, a one-dimensional DP with a limited number of system operation modes is implemented.

Also, different energy management objectives have been selected such as minimizing the micro-grid operation cost [41], maximizing the revenue due to the electricity market price [42], minimizing micro-grid operation effect on the main grid [43], improving power quality [44], safety and reliability [45]. However, most of the above-mentioned optimization techniques need either computationally expensive efforts which makes them unsuitable for real-time applications or specific solvers [37]. Therefore, a combination of the real-time rule-based controller along with an off-line optimization technique is recommended and is used in this paper.

This paper proposes a two-scale energy management unit (EMU) for a magnetically coupled residential smart micro-grid. Utilizing the magnetic bus leads to a more flexible power flow control, a larger number of operation modes, and less control complexity compared to the previously reported micro-grids. The main contributions of the paper can be listed as the following:

- Proposing a two-scale EMU containing a real-time fuzzy controller and a long-term predictive controller based on a novel variable-step size two-dimensional dynamic programming (2D-DP) technique. Therefore, both the real-time condition and the long-term predictions of the energy generation and consumption have been taken into account.
- The inclusion of more effective parameters in the energy management process compared to the previously reported researches to the best of authors' knowledge. The main parameters are the real-time and predicted profile of the grid electricity price, load power demand and PV power generation; efficiency performance of the battery and converters according to their power flow; micro-grid topology (based on power balance equations); energy cost of the PV and fuel cell considering their capital and running costs; operating limits of the micro-grid elements such as electrical power and current ratings.
- Providing a detailed study on the technical points of energy management and control of the micro-grids with a large number of operation modes including real-time control, mode selection strategy and mitigating transient oscillations by using hysteresis based fuzzy membership functions and defining bridging modes.

Due to the nonlinear nature of the micro-grid elements, a large number of operation modes (totally 20 different grid-connected and off-grid operation modes) and system statuses, using rule-based control methods increases the control complexity. The fuzzy controller is prefered as only the main rules and selected operation modes can be grasped which simplifies the control process. The common optimization methods using linear and quadratic programming techniques result in extensive computational efforts and require relaxation techniques due to the presence of nonlinear and integer variables. Therefore, the 2D-DP technique is used to optimally manage the battery state of charge (SOC) and fuel cell state of hydrogen (SOH) according to the long-term energy plans. To reduce the computation time and increase the accuracy of the optimization method, shorter step sizes are allocated to the more accurate prediction times. To smooth the mode transition and reduce the oscillation of the system during the mode transition, hysteresis-based fuzzy membership functions are introduced, and appropriate mode transition strategy is designed. The proposed EMU is tested experimentally for three different energy management scenarios. Energy distribution and cost analysis are provided.

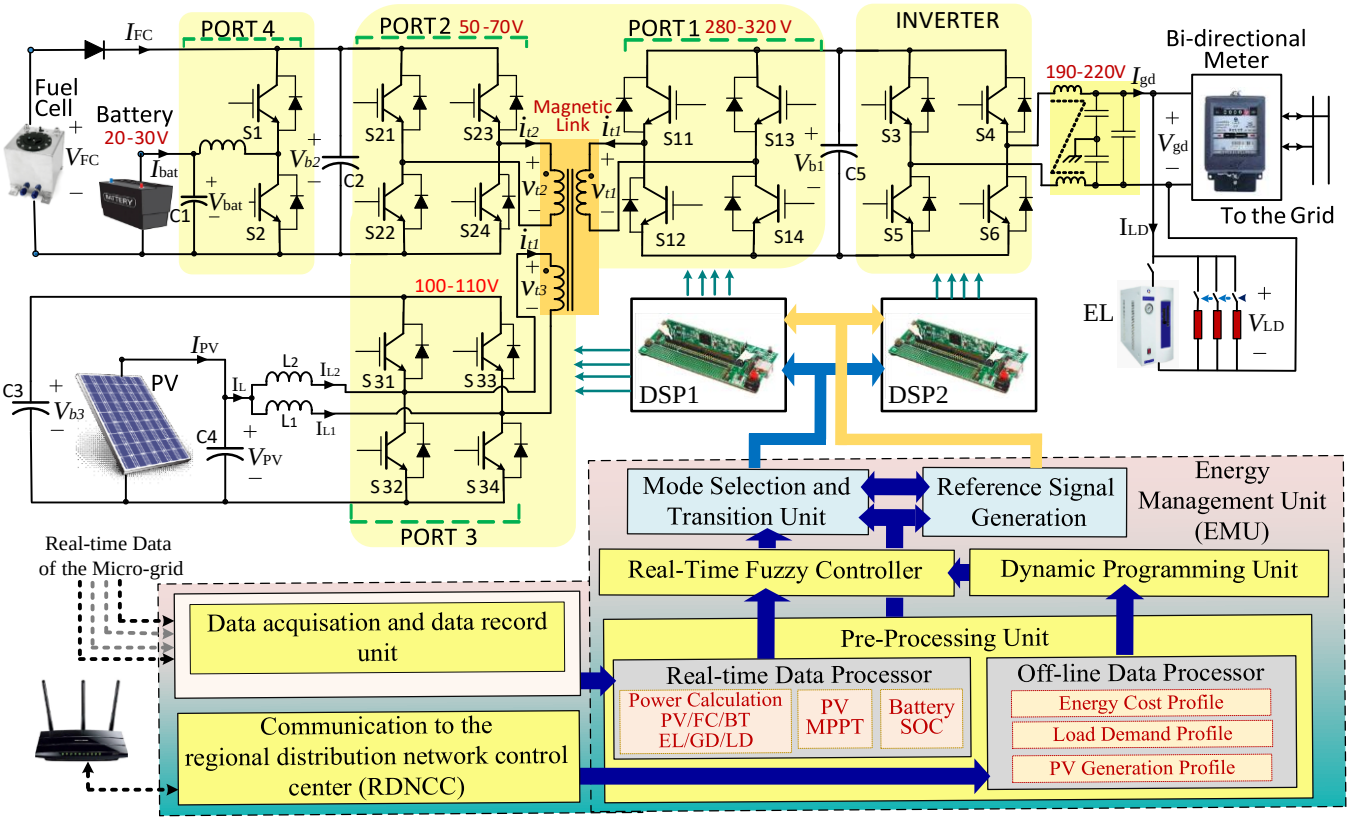

Fig.1. Structure of the proposed smart micro-grid and energy management unit (EMU)

The rest of the paper is organized as follows. The structure of the proposed micro-grid is reviewed in section II. The EMU operation and energy management technique are studied in section III. The experimental test results and conclusions are presented in sections IV and V respectively.

II. Structure of the Proposed Micro-Grid

The electrical schematic of the proposed micro-grid and controllers are presented in Fig.1. As can be seen, the micro-grid is designed to integrate the energy of a PV array, a fuel cell stack and a battery as storage device to supply a residential load. The system includes three H-bridge dc-ac converters (presented as port one, two and three) linked to a multi-winding transformer as a magnetic bus to form a triple active bridge (TAB) phase-shift converter. It can also operate as a dual active bridge (DAB) converter when power is transferred only between the port two or three to port one. The dc bus in port two (V_{b2}≈50-70 V) is directly supplied by fuel cell or through a bidirectional buck-boost converter by a battery bank (V_{bat}≈20-24V). The battery is charged in the buck mode and discharged into the bus in the boost mode. It also is used in standby mode when the fuel cell is activated to compensate for the slow dynamic response of the fuel cell. In the port three, the PV output voltage is boosted by an interleaved boost converter to the dc bus level (V_{b3}≈100-110V). The switching devices S_{31}-S_{34} are shared between H-bridge converter and interleaved boost converter in port three and capacitor C_3 is used as an energy buffer. The voltages V_{b2} and V_{b3} are converted to high-frequency ac square waves by using the H-bridge converters of port two and three respectively and linked to the windings of the magnetic link.

The H-bridge unit in port one, generates a dc high-voltage (V_{b1}=280-320V), from the high-frequency voltage induced in winding one. A bidirectional single-phase inverter changes the resultant dc voltage to a low frequency (50 Hz) ac voltage which is further used to supply the residential load or transfer to the utility grid. The inverter can be used in reverse direction as a rectifier to transfer the grid energy to the high voltage dc bus and charge the battery using ports one, two and four simultaneously. The power flow between the converter ports is controlled by leading or lagging the generated ac voltages in ports two and three respected to port one (φ_{21} and φ_{31} respectively) according to the phase shift control technique [20], [21].

An electrolyzer is used as an optional load to produce hydrogen for fuel cell and also increase the system's energy storage flexibility. As can be seen, the residential load is always connected to the main grid. The entire micro-grid system is controlled by two digital signal processors (DSPs) as local controllers. The voltage and current control systems have been implemented in local controllers for all converters using proportional-integral (PI) controllers and the pulse width modulated (PWM) drive signals are generated for switching devices. On the other hand, a computer (laptop) is used as a master controller to determine the appropriate operation mode and perform the energy management. More details on the device level controllers remain for future publications.

III. Energy Management Technique

The EMU operates as an intermediate control level between regional distribution network control centre (RDNCC) and device level controllers. The EMU block diagram and operational units are presented in Fig.1. As can be seen, the input signals to the EMU including voltage and current of all converter ports and user-defined settings are input to the data acquisition and record unit. On the other

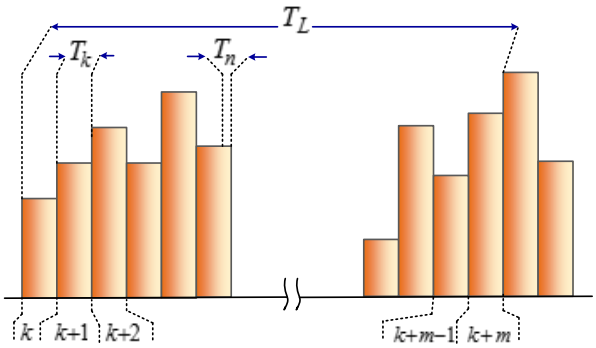

Fig.2. Definition of the sampling times in the EMU

hand, the grid energy cost profile, grid energy transfer control signals and the metrological data for PV generation and load demand forecasts are received from communicating to the RDNCC. A pre-processing unit including a real-time and an off-line processor is designed to prepare the required data for the controllers. The sampling times assigned to each control level are presented in Fig.2 and are used as a reference throughout the paper. The forecasted data for the moving time-frame T_L (ranges from minutes to hours) is regularly updated with the sampling time T_k. However, the real-time data input to the data acquisition unit is updated with the sampling time T_n (ranges from milliseconds to seconds). Both T_k and T_n are much more than local processors sampling time T_s (ranges in microseconds).

A. Operation of Pre-processing Unit

The real-time data of micro-grid parameters (voltage and current samples) are sent to the real-time data processor to calculate the components power, estimate the battery SOC and the fuel cell SOH, and perform the maximum power point tracking (MPPT) of the PV port. The fuel cell (FC) power $P_{FC}(n)$, for each sampling time n, is calculated by multiplying the fuel cell voltage $V_{FC}(n)$ and current $I_{FC}(n)$. The battery (BT), load (LD), electrolyzer (EL), grid (GD) and PV powers are calculated similarly using their voltage and current samples. The battery SOC is defined from

$$SOC(n) = SOC(n-1) + \frac{T_n}{C_{BT}}\left[I_{BT}(n) - I_{BT}(n-1)\right] \quad (1)$$

where $I_{BT}(n)$ is the battery current at the n-th sampling time which can be positive or negative during the charge or discharge respectively and C_{BT} the nominal capacity of the battery bank. The state of hydrogen, $SOH(n)$ is estimated using signals received from the sensors installed in the hydrogen tank. The MPPT process is performed using $I_{PV}(n)$ and $V_{PV}(n)$ according to a variable step size incremental conductance (INC) method and is sent to the reference signal generation unit. The real-time value of the difference between PV power generation $[P_{PV}(n)]$ and the load demand $[P_{LD}(n)]$ and the difference between fuel cell energy cost $[C_{FC}(n)]$ and grid energy cost $[C_{GD}(n)]$ required for the real-time fuzzy controller are determined from

$$\Delta P(n) = P_{LD}(n) - P_{PV}(n), \quad \Delta C(n) = C_{GD}(n) - C_{FC}(n) \quad (2)$$

where C_{GD} is equal to C_{GD_sell} for selling power to the grid and C_{GD_buy} for purchasing from the grid. On the other hand,

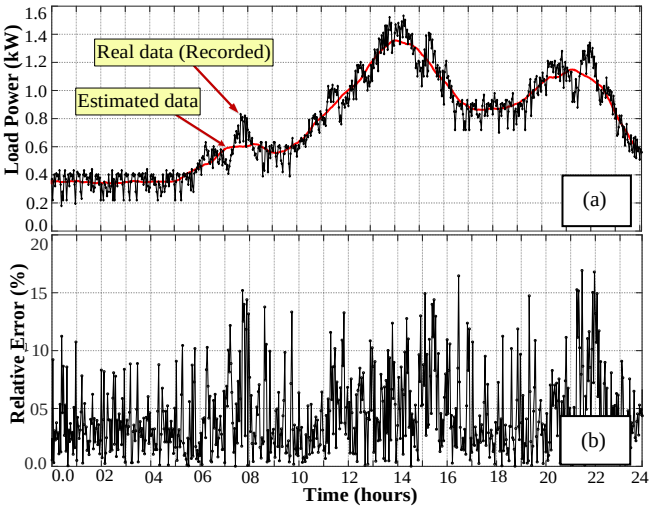

Fig.3. (a) Comparison of measured and estimated Load power demand for 24h-ahead, and (b) relative error between measured and estimated values

the data received from the communication unit is sent to the off-line pre-processing unit. The metrological data along with the previously recorded data for the days under the same weather condition is used to forecast the PV power generation profile for the next moving time frame T_L. The resultant continuous profile of $\tilde{P}_{PV\text{-}24h}(t)$, is discretised for the sampling times T_k, to simplify the analysis of the predicted data and speed up the decision making process from

$$\tilde{P}_{PV\_24h}(k) = \frac{1}{T_k}\int_{t_0+kT_k}^{t_0+(k+1)T_k} \tilde{P}_{PV\_24h}(t)dt \quad k \in (0,1,2,\ldots,\frac{24hours}{T_k}-1) \quad (3)$$

where t_0 is the prediction starting time [31]. The forecasted profile of the load demand is obtained from the average of load demand for the past 30 days with similar conditions using recorded data. The forecasted and actual data of the load demand for a typical day are compared in Fig.3. As can be seen, the resultant relative error for a complete day is always less than 15 %. On the other hand, it is assumed that the EMU receives the updated profiles of the electricity price of the grid from the RDNCC regularly. The fuel cell cost is an almost constant value and evaluated by the consumer according to the running cost, efficiency, and capital cost. The discretised profiles are further used by the dynamic programming unit.

B. Operation of Dynamic Programming Unit

The main task of the long-term energy management is to determine the best variation route of the available capacity of storage devices (i.e. ΔSOC for battery and ΔSOH for hydrogen tank) during the next moving time-frame to meet the energy management objectives. The resultant values then are sent to the real-time fuzzy controller to determine the next operation mode of the system accordingly. In this paper, the 2D-DP method is used to optimally manage the available capacity of storage devices as using conventional rule-triggered energy management methods restricts the system flexibility and does not guarantee the optimal operation due to a large number of operation modes. The DP is a graph-based optimisation technique which defines the best variation schedule of the system variables during a moving time-frame according to a pre-defined objective

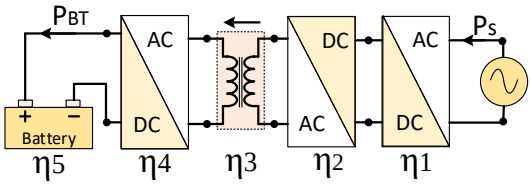

Fig.4. Schematic of a the grid-connected battery system

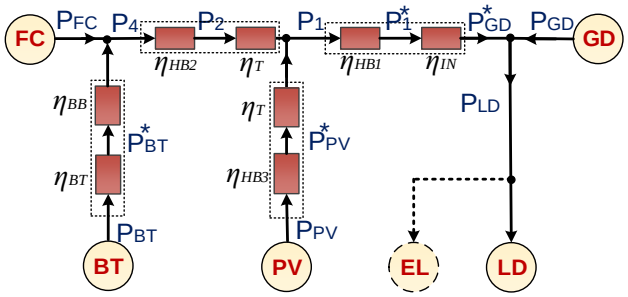

Fig.5. Simplified power flow model of the micro-grid

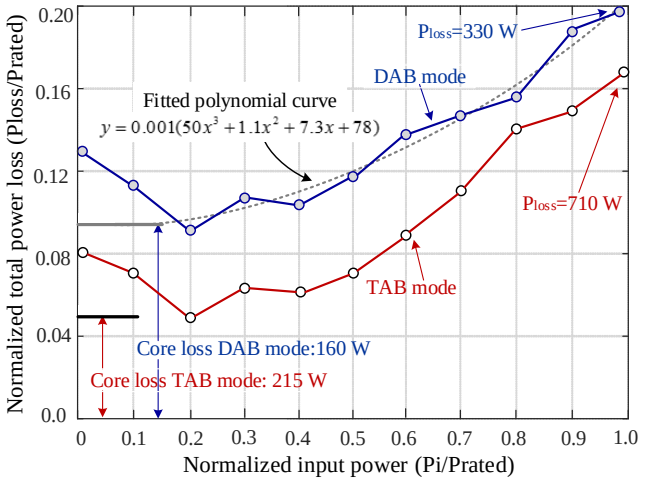

Fig.6. The normalized power loss of the converters and the magnetic link to the rated power for two cases of DAB and TAB operation modes and the fitted polynomial curve

function [37]. The time-frame is divided into small time-steps, and positive or negative changes are applied to the variables in each step, and the system status is evaluated accordingly considering the system features and constraints. The sequential process of variation and evaluation is performed for all steps of the time-frame and is known as a variation path. The process is then completed by evaluation of all possible paths to find the path with the best satisfaction of objective function. The advantage of the method is that the constraints and the performance index can be linear or non-linear, convex or concave [37]. However, it needs a large memory space and computation efforts in the case of long time-frames with short time-steps.

In this paper, the control objective is to manage the storage devices capacity in such a way that minimizes the customer's energy bill by proper arrangement of selling/buying energy to/from the grid. In this regard, several factors need to be taken into account. The efficiency characteristics of the converters and micro-grid elements are an important factor in the economic operation of the micro-grid. As an example in Fig.4, the battery is planned to receive energy from the grid at off-peak and sell it at the peak demand time. Assuming that all conversion units including the battery have an equal efficiency η=0.95, then

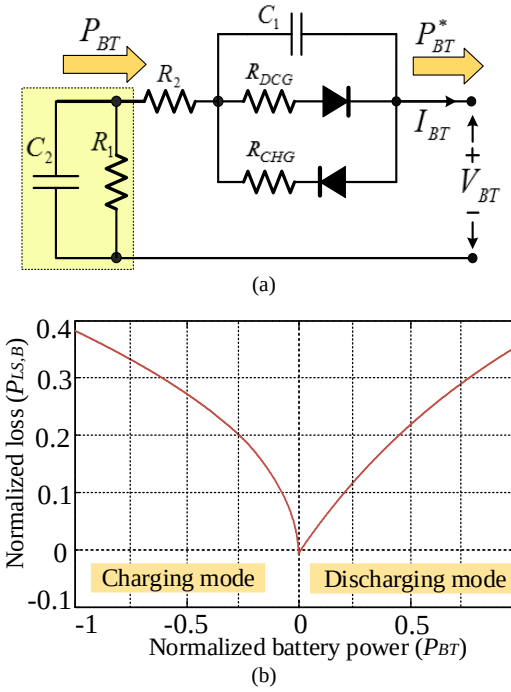

Fig.7. (a) Equivalent model and (b), charge and discharge loss characteristics of the battery

the feed-in tariff should be at least 1.7 times of the purchasing cost for economic operation of the system. Therefore, the efficiency performance of the converters and battery loss are included in the optimization process. On the other hand, the physical constraints of the micro-grid elements should be taken into account. Fig.5 illustrates the simplified power flow model of the system including the converter blocks and the micro-grid components. The power balance equations in the micro-grid according to the presented model are selected as the main physical constraints.

$$P_{FC} + P_{PV} + P_{BT} + P_{GD} - P_{LD} - P_{LS} = 0 \quad (4)$$

$$P_{LS} = P_{LS,T} + P_{LS,C} + P_{LS,B} \quad (5)$$

$$P_{LS,C} = P_{LS,BB} + P_{LS,HB1} + P_{LS,HB2} + P_{LS,HB3} + P_{LS,IN} \quad (6)$$

where P_{LS}, $P_{LS,T}$, $P_{LS,C}$ and $P_{LS,B}$ are the power losses in the entire micro-grid system, transformer, the converters and the battery respectively. The power loss in the converters is mainly related to the switching and conduction losses in the H-bridge converters ($P_{LS,HB}$), buck-boost converter ($P_{LS,BB}$) and inverter ($P_{LS,IN}$). To simplify the analysis and modeling of the losses using experimentally measured data, the efficiency blocks of the transformer and the H-bridge converters in port two and three are combined. The resultant normalized efficiency curve is determined for both cases of DAB and TAB operation modes as presented in Fig.6. To estimate the power loss of each operation mode, a third-order polynomial is determined by interpolation of the experimentally measured efficiency curves. The low input power range (p_{in}/p_{rated}=0.1- 0.2) where power loss increases slightly (due to the incomplete ZVS and increasing snubber loss) is not included in the curve fitting. On the other hand, the power loss in the battery during the charge and discharge processes should be taken into account. The battery model and the normalized loss as a function of battery power (P^*_{BT}) are illustrated in Fig.7. As can be seen, the energy

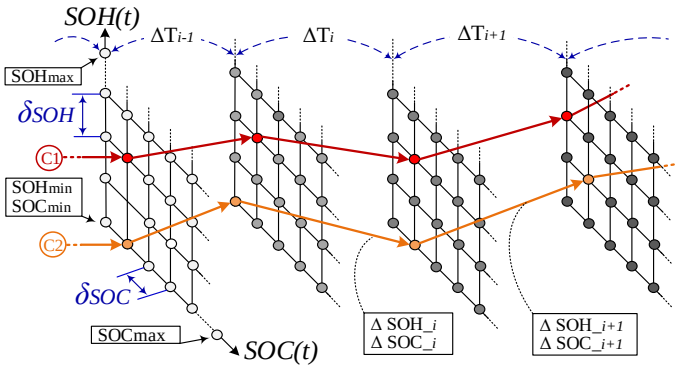

Fig.8. Trajectory of 2D dynamic programming and two possible paths (C1 and C2)

losses during the charge and discharge process are not equal and therefore, different resistances are considered to model for charge and discharge losses. The energy loss due to the battery self-discharge is ignored ($R_1 \approx \infty$). The battery efficiency during the charge (η_{BT}^{CHG}) and discharge (η_{BT}^{DCG}) process is determined as [46]:

$$\eta_{BT}^{CHG} \approx (\eta_{BT}^{DCG})^{-1} = \frac{P_{BT}}{P_{BT}^{*}} = 1 - \left| \frac{V_{OC} - \sqrt{V_{OC}^2 - 4RP_{BT}^{*}}}{2V_{OC}} \right| \quad (7)$$

where P_{BT} is the battery cells power, P_{BT}^{*} the battery terminal power, R the charge or discharge loss resistor and V_{OC} the battery open-circuit voltage. There are some other constraints related to the battery and fuel cell such as SOC variation range allocated for each operation mode, charging and discharging power limits, fuel cell power range for operating in the linear (ohmic polarization) area, and the power transfer limits to/from the grid. These constraints can be presented as:

$$SOC_{\max} < SOC < 1 \Rightarrow Bus\ \ voltage\ \ stabilization \quad (8)$$

$$SOC_{med} < SOC < SOC_{\max} \Rightarrow Energy\ \ storage\ \ and\ \ stabilization \quad (9)$$

$$SOC_{\min} < SOC < SOC_{med} \Rightarrow Off - Grid\ \ application \quad (10)$$

$$P_{BT} \le P_{BT,\max}\ ,\ \ P_{GD} \le P_{GD,\max} \quad (11)$$

$$P_{FC,\min} < P_{FC} \le P_{FC,\max}\ ,\ \ P_{EL} \le P_{EL,\max} \quad (12)$$

where SOC_{min}, SOC_{med} and SOC_{max} are the minimum, medium and maximum of the battery SOC levels and equal to 0.9, 0.4, and 0.1 respectively. $P_{BT,max}$, $P_{GD,max}$ and $P_{EL,max}$ are the maximum power of the battery, grid and electrolyzer. $P_{FC,min}$ and $P_{FC,\ max}$ are the maximum and minimum of the fuel cell power respectively. The trajectory of the 2D-DP problem is presented in Fig.8 and the main stages of the process are illustrated in the flowchart in Fig.9. The moving time-frame T_L is divided into m steps represented as ΔT_i . The problem for each time step ahead (ΔT_i), starts with the applying a change (positive or negative) to the SOC and SOH, presented as δSOC and δSOH respectively as system variables. For constant time steps ΔT_i , the value of δSOC and δSOC remains constant. However, a variable step size process with more concentration on the time-steps closer to the actual time is used in this paper. This makes the process more effective and accurate and reduces the total computation time. Applying a positive δSOC means that the battery should be in charging mode, negative in discharging mode and zero in standby mode. On the other hand,

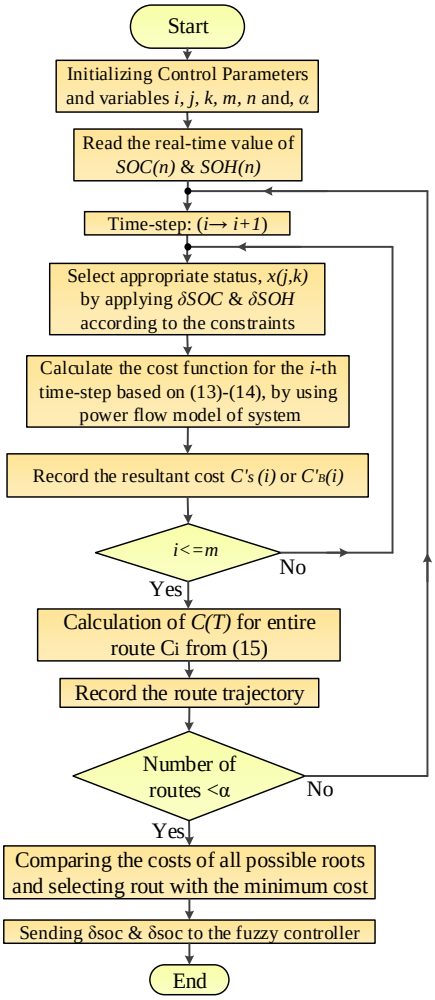

Fig.9. Flowchart of the main steps of the proposed 2D dynamic programming-based energy management where $x\ (i, j, k)$ denotes the state variable of the system at time step (i). In this diagram, i , j and, k are the iteration variables of the time-step, the SOC levels and the SOH levels respectively. Furthermore, m equals the total number of the time-steps in a moving time-frame, and α the total number of possible routes.

applying positive δSOH means an active electrolyzer, negative an active fuel cell and zero means both should be off. The amounts of P_{BT}, P_{EL} and P_{FC} are estimated accordingly taking into account the constraints in (11) and (12). The PV power generation (P_{PV}) and load demand (P_{LD}) are also obtained using the forecasted profiles generated in the off-line data processor. The power transfer to/from the grid (P_{GD}) and the power loss in the system (P_{LS}) then can be easily found using (4)-(6) based on the power flow model of the system presented in Fig.5. Considering the grid energy cost profile received from RDNCC, the benefit from selling energy to the grid C_S, and the expense of buying energy from the grid C_B, are calculated from:

$$C_S^i = \left[P_{GD}^i * C_{GD\_Sell}^i * \Delta T_i \right],\ \ if\ \ P_{GD}^i \langle 0 \quad (13)$$

$$C_B^i = \left[P_{GD}^i * C_{GD\_Buy}^i * \Delta T_i \right],\ if\ \ P_{GD}^i \rangle 0 \quad (14)$$

where C_{GD_Buy} is the cost of the energy received from the grid and C_{GD_Sell} , the energy sold to the grid at i-th time-step. The energy cost of the m-th path then is obtained from the summation of the energy cost of all included time-steps from

$$C(T) = \sum_{i=1}^{m} \left[C_S^i + C_B^i \right] \quad (15)$$

TABLE.I. FUZZY CONTROL RULES

Grid-connected rules

INPUT VARIABLES				OUTPUT VARIABLE			
ΔP(*n*)	ΔC(*n*)	ΔSOC	ΔSOH	BT	FC	EL	P_{GD}
PL	PL	PL	PL	CD	OFF	OFF	NL
PL	PL	PL	PS	CD	ON	OFF	MD
PL	PL	ZE	PL	CD	OFF	OFF	NL
PL	PL	ZE	PS	CD	ON	OFF	MD
PL	PL	NL	PL	DO	OFF	OFF	MD
PL	PL	NL	PS	DO	ON	OFF	MD
PL	ZE	PL	PL	CO	OFF	OFF	NL
PL	ZE	PL	PS	CO	ON	OFF	NL
PL	ZE	ZE	PL	DO	OFF	OFF	MD
PL	ZE	ZE	PS	DO	ON	OFF	MD
PL	ZE	NL	PL	DO	OFF	OFF	NL
PL	ZE	NL	PS	DO	ON	OFF	MD
PL	NL	PL	PL	CO	OFF	ON	NL
PL	NL	PL	PS	CO	OFF	OFF	NL
PL	NL	ZE	PL	CD	OFF	ON	NL
PL	NL	ZE	PS	CD	OFF	OFF	NL
PL	NL	NL	PL	DO	OFF	ON	NL
PL	NL	NL	PS	DO	OFF	OFF	NL
ZE	PL	PL	PL	CD	OFF	OFF	MD
ZE	PL	PL	PS	CO	ON	OFF	MD
ZE	PL	ZE	PL	CD	OFF	OFF	MD
ZE	PL	ZE	PS	CD	ON	OFF	PL
ZE	PL	NL	PL	DO	OFF	OFF	PL
ZE	PL	NL	PS	DO	ON	OFF	PL
ZE	ZE	PL	PL	CD	OFF	OFF	MD
ZE	ZE	PL	PS	CO	ON	OFF	MD
ZE	ZE	ZE	PL	CD	OFF	OFF	MD

INPUT VARIABLES				OUTPUT VARIABLE			
ΔP(*n*)	ΔC(*n*)	ΔSOC	ΔSOH	BT	FC	EL	P_{GD}
ZE	ZE	ZE	PS	CD	OFF	OFF	MD
ZE	ZE	NL	PL	CD	OFF	OFF	MD
ZE	ZE	NL	PS	CD	OFF	OFF	MD
ZE	NL	PL	PL	CO	OFF	ON	NL
ZE	NL	PL	PS	CO	OFF	OFF	NL
ZE	NL	ZE	PL	CD	OFF	ON	NL
ZE	NL	ZE	PS	CD	OFF	OFF	MD
ZE	NL	NL	PL	CD	OFF	ON	NL
ZE	NL	NL	PS	CD	OFF	OFF	MD
NL	PL	PL	PL	CO	OFF	OFF	MD
NL	PL	PL	PS	CO	ON	OFF	PL
NL	PL	ZE	PL	CD	OFF	ON	MD
NL	PL	ZE	PS	CD	ON	OFF	PL
NL	PL	NL	PL	DO	OFF	ON	PL
NL	PL	NL	PS	DO	ON	OFF	PL
NL	ZE	PL	PL	CO	OFF	OFF	MD
NL	ZE	PL	PS	CO	OFF	OFF	MD
NL	ZE	ZE	PL	CD	OFF	ON	MD
NL	ZE	ZE	PS	CD	OFF	OFF	PL
NL	ZE	NL	PL	DO	OFF	ON	MD
NL	ZE	NL	PS	DO	OFF	OFF	PL
NL	NL	PL	PL	CO	OFF	ON	MD
NL	NL	PL	PS	CO	OFF	OFF	MD
NL	NL	ZE	PL	CD	OFF	ON	MD
NL	NL	ZE	PS	CO	OFF	OFF	PL
NL	NL	NL	PL	DO	OFF	ON	MD
NL	NL	NL	PS	CD	OFF	OFF	PL

Off-grid rules

INPUT VARIABLES			OUTPUT VARIABLE			
ΔP(*n*)	ΔSOC	ΔSOH	BT	FC	EL	LD_{DMP}
PL	PL	PL	CD	OFF	OFF	OFF
PL	PL	PS	CD	ON	OFF	OFF
PL	ZE	PL	DO	OFF	OFF	OFF
PL	ZE	PS	DO	ON	OFF	OFF
PL	NL	PL	DO	OFF	OFF	OFF
PL	NL	PS	DO	ON	OFF	OFF
ZE	PL	PL	CD	OFF	OFF	OFF
ZE	PL	PS	CD	ON	OFF	OFF
ZE	ZE	PL	CD	OFF	OFF	OFF

INPUT VARIABLES			OUTPUT VARIABLE			
ΔP(*n*)	ΔSOC	ΔSOH	BT	FC	EL	LD_{DMP}
ZE	ZE	PS	CD	ON	OFF	OFF
ZE	NL	PL	DO	OFF	OFF	OFF
ZE	NL	PS	DO	ON	OFF	OFF
NL	PL	PL	CO	OFF	OFF	OFF
NL	PL	PS	CO	OFF	OFF	OFF
NL	ZE	PL	CO	OFF	OFF	OFF
NL	ZE	PS	CO	OFF	OFF	OFF
NL	NL	PL	DO	OFF	ON	OFF
NL	NL	PS	CD	OFF	OFF	ON

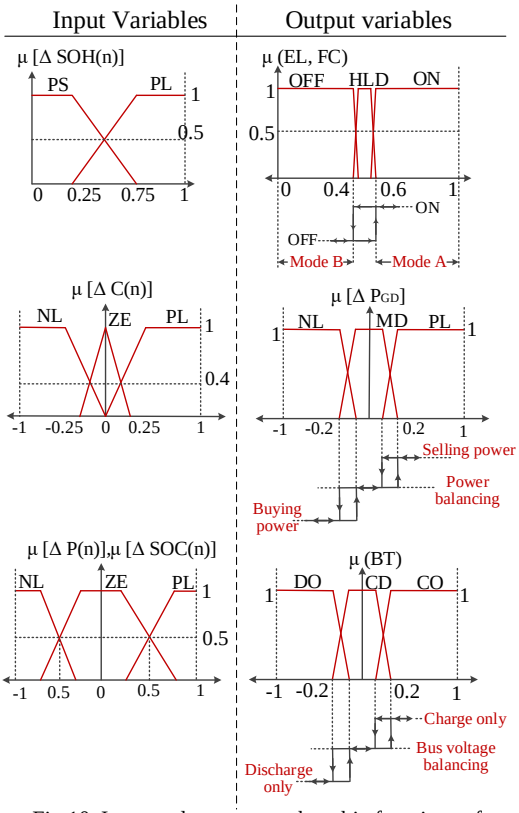

Fig.10. Input and output member ship functions of the fuzzy controller

Finally, to find the path with the minimum cost, the energy cost of all possible paths are compared. It should be noted that the number of possible paths reduces considerably as the number of possible states for each step change is limited due to the *δSOC* and *δSOH* limits. As shown in Fig.8, C1 and C2 are examples of two possible paths. The resultant change in the *SOC* and *SOH* according to the selected path (Δ*SOC* and Δ*SOH*) is normalized and sent to the real-time fuzzy controller to be used in the decision-making process.

C. The Real-time Fuzzy Controller

The fuzzy controller determines the status of the micro-grid elements (fuel cell, electrolyzer and battery) and the amount of power can be received from or supplied to the grid taking into account Δ*SOC* and Δ*SOH* received from DP unit and the real-time values of the power difference [Δ*P(n)*] and energy cost difference [Δ*C(n)*]. The variables Δ*SOC(n)* and Δ*SOH (n)* are used to determine the battery and fuel cell/electrolyzer statuses respectively, Δ*C(n)* to compare the fuel cell and the grid energy costs. Δ*P(n)* represents the difference between PV generation and load demand and is used to determine the source that can supply or absorb it. Fig.10 shows the normalized input and output membership functions. The input membership functions are classified as negative large (NL), negative small (NS), zero (ZE), positive small (PS), and positive large (PL). On the other hand, the status of the fuel cell, battery, electrilyzer and grid conversion ports are selected as the output variables. The fuel cell and electrolyzer status is in the form of ON and OFF, and the function HOLD is considered as a hysteresis function to reduce the mode fluctuations in the boundary conditions. The battery status functions are selected as charge only (CO), discharge only (DO) or charge and discharge (CD). The energy transfer to/from the grid is classified as negative large (NL) for receiving energy, medium (MD) for flexible transfer to/from the grid, and positive large (PL) for sending energy to the grid. Table.I illustrates the fuzzy control rules for the grid-connected and off-grid operation conditions. As can be seen, in general, the small values of the difference between the PV generation and load demand is covered by the battery and/or grid depending on the value of Δ*SOC* received from DP unit and the cost of energy. When the difference is more than the battery capacity and less than the fuel cell, it should be covered by either grid or fuel cell considering the energy cost taking into account the constraints in (8)-(12) for each sampling time. In the case of off-grid operation, Δ*C(n)* is not considered as input variable due to the absence of the grid energy and the fuel cell energy cost assumed more than the battery. Furthermore, a dump load (LD_{DMP}) is considered as output to absorb the surplus energy and can be a water

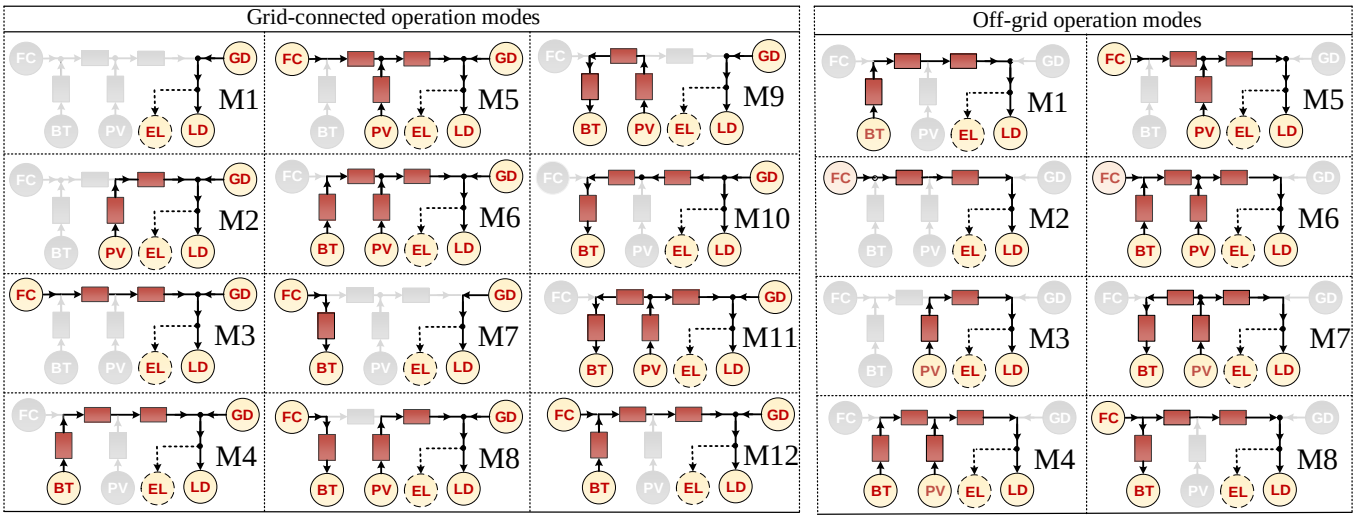

Fig.11 The grid-connected and off-grid operation modes of the proposed micro-grid

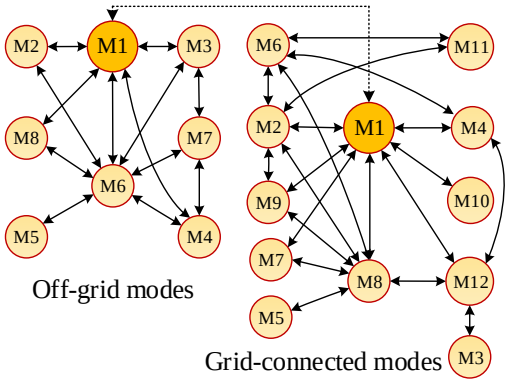

Fig.12 Schematic of the designed state transition diagram (STD)

heating system for more efficient energy use. The max-min product inference technique and the centre of gravity defuzzification method are used to determine the outputs of the fuzzy controller. The hysteresis functions are applied to the output membership functions to reduce the undesirable oscillations in the operating modes. As a result, any change in the output variables at the boundary of two adjacent statuses should exceed a threshold level (determined by the hysteresis band) to result in a change in the micro-grid operation mode. The resultant output signals related to the operation status of the battery, fuel cell and electrolyzer and the range of power that can be sent to, or received from the grid are sent to the mode selection and transition unit (MSTU) to extract the appropriate operation mode as will be discussed in the next section.

D. Mode Selection and Transition Unit

The proposed micro-grid can operate in 12 grid-connected and 8 islanded modes as presented in Fig.11. The operation modes are presented based on the power flow model of the micro-grid illustrated in Fig.5. Due to the large number of operation modes and converters in the proposed micro-grid, the MSTU is designed to manage and smooth the mode variation process. The mode transition process should follow several practical stages including evaluation of destination mode conditions, sending the proper reference signals to the local controllers, soft start operation (depending on the mode) and checking the final status of the system in the new mode. Performing these stages takes some time (between 50 ms to 200ms depending on the modes) and may need to activate or deactivate H-bridge converters. However, the voltage of the high-voltage and low-voltage dc busses should be kept constant to avoid any possible interruption in the system operation. Due to this, the bridging modes are defined as when the battery and grid as flexible bidirectional energy sources of the system in the off-grid and grid-connected conditions are supplying the dc bus. Therefore, the mode transition can happen directly between the modes or indirectly using a bridging mode.

A state transition diagram (STD) is designed for both grid-connected and off-grid condition to determine the proper transition path between the modes as presented in Fig.12. As the load is always connected to the grid, this case is selected as the basic mode (M1) in grid-connected condition and is used as bridging mode in most of the transition paths. On the other hand, the load is always supplied by the battery in off-grid condition and therefore, it is selected as basic mode (M1). In addition, a mode transition diagram defines the details of the transition condition and stages including detection of mode-change, evaluation of the destination mode condition and generation of reference signals for local controllers.

IV. Experimental Test of the Proposed EMU

A prototype of the proposed micro-grid is implemented for a 4.5 kW, 20 kWh/day residential load as presented in Fig.13.The Texas instrument DSPs (TMS320F28335) are used as local controllers. A laptop is used as a master controller to perform the energy management and operation mode control using a MATLAB graphical user interface (GUI). The experimental waveforms of the micro-grid converters (referring to Fig.1) for operating condition selected as: P_{PV}=250 W, P_{FC}=550 W, P_{gd}=750 W, V_{PV}=20 V, V_{b2}=65 V, V_{b3}=110 V, V_{b1}=300 V, $\varphi_{21}=\pi/3$ and $\varphi_{31}=\pi/6$ where φ_{21} and φ_{31} are the phase shift angles of the fuel cell and the PV ports to the inverter port. Fig.14 (a) shows the high-frequency voltages generated by H-bridge units and the related currents flowing through the transformer.

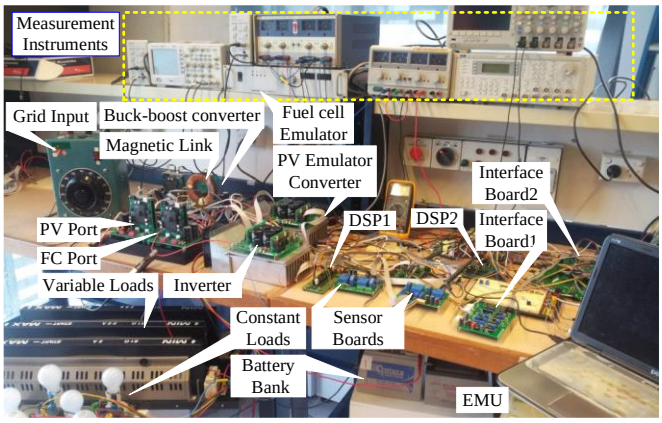

Fig.13. The experimentally developed residential micro-grid

The leading phase shit angles of φ_{21} and φ_{31} are presented on the waveforms. Fig.14 (b) illustrates the currents in the inductors L1 and L2 and the total current of the interleaved boost converter. The resultant current then is filtered by C3 as the PV output current. Fig.14(c) illustrates the voltage and current of the single-phase inverter in the inverting and rectifying modes. As can be seen, the power in the rectifier mode (400 W) flows in the opposite direction and is used to charge the battery. As can be seen the THD of the current in both cases is in the standard range for the grid-connected residential systems (less than 5 %). Fig.15 shows the flowchart of mode transition process performed by MSTU. As can be seen, the main stages include evaluation of the mode transition condition, definition of mode transition path and bridging mode according to the STD, setting up the proper reference signals for the local controllers and soft starting process. Fig.16 illustrates the change in the power profiles of the micro-grid elements at the mode transition instants for three different cases. In the first case, the operation mode is changed from M5 to M3 where M8 and M12 are used as bridging modes according to the STD presented in Fig.12. The battery is used as a bus voltage stabilizer when the PV power is approached to zero and the fuel cell undertakes to supply the difference. In the second case, the operation mode is changed from M2 to M11 through a direct transition. The PV power increases to more than load demand and the grid requirement. The surplus energy then is sent to the battery after transition delay. The third case presents a transition in off-grid condition where the PV power which is supplying the load in mode M3, drops to zero. Therefore, the fuel cell undertakes the role to supply the load in mode M2 and the battery is activated during the bridging mode M6 to compensate for the slow dynamic response of the fuel cell. As can be seen the entire transition process takes about 230 ms.

To validate the operation of the EMU, a residential load is modelled by parallel connection of two groups of variable and constant loads as presented in Fig.13. The experimental test is carried out for a 2 hours time duration to model a residential load daily profile starting at 12 AM (720 samples with time duration of 10 seconds) and T_L=40 min, T_k=10s and T_n=100 ms. The PV power generation profiles for sunny and cloudy weather conditions are considered. The energy supplied or received by each element x, can be easily obtained by using its discretised daily power profile $P_x(k)$, and the sampling time T_k from

$$E_{x\_24h} = \sum_{k=1}^{720} P_{x\_24h}(k)T_k = T_k \sum_{k=1}^{720} P_{x\_24h}(k) \quad (16)$$

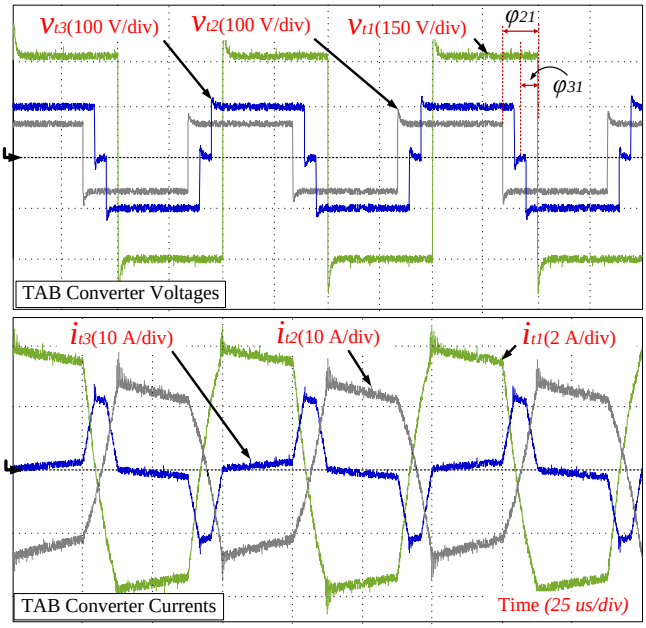

(a)

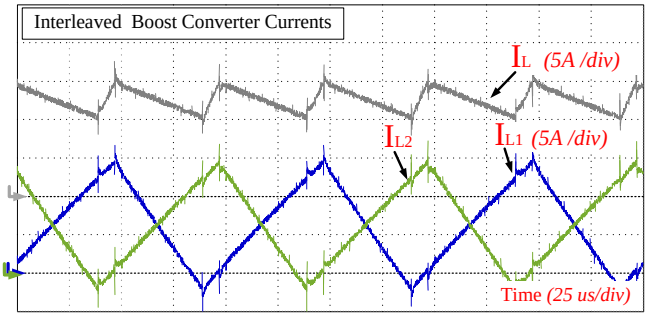

(b)

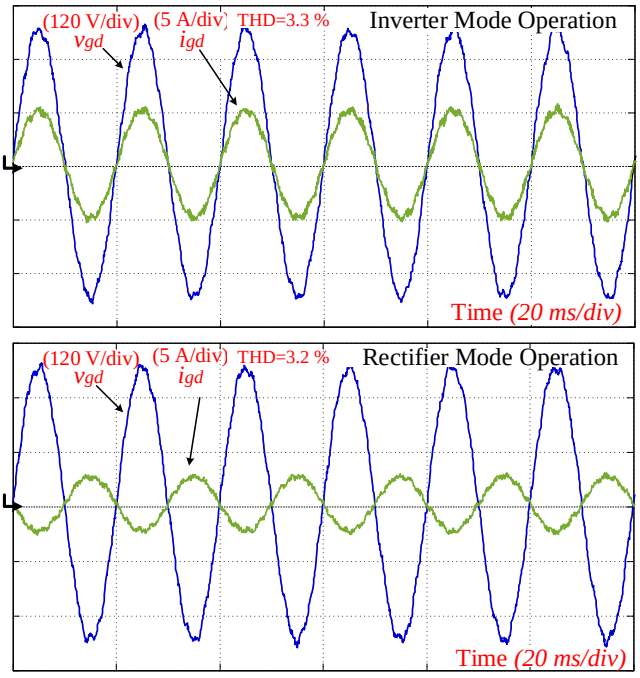

(c)

Fig.14. The experimentally measured waveforms of the micro-grid converters , (a) the TAB converter voltages and currents for (b) the interleaved boost converter currents and, (c) the single-phase inverter output in inverting and rectifying operation conditions.

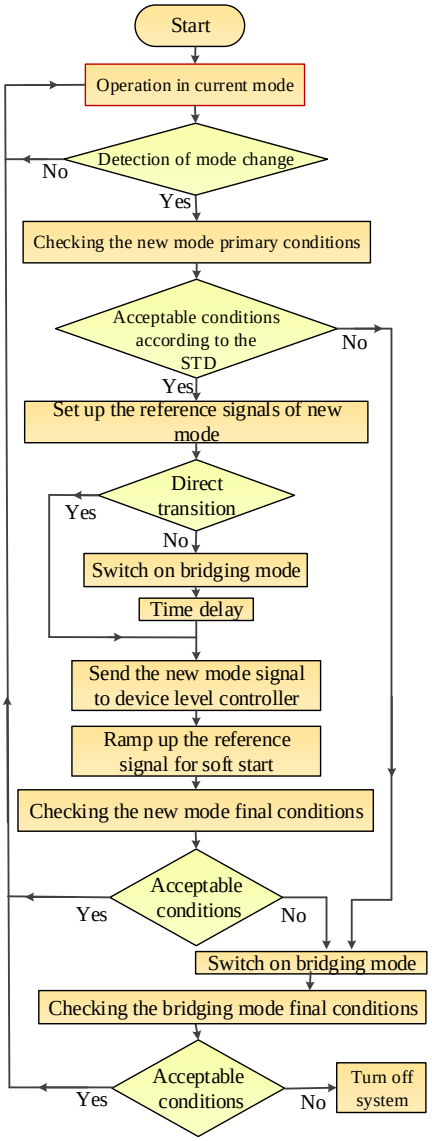

Fig.15. Flowchart of mode transition process

where x can be PV, EL, FC or LD. The energy received by the battery in charging ($E_{BT\_24h}^{CHD}$), or supplied in discharging ($E_{BT\_24h}^{DCH}$) modes, and sold to the grid ($E_{GD\_24h}^{SEL}$) or supplied by the grid ($E_{GD\_24h}^{BUY}$) are defined similarly. The total energy loss in the system (E_{LS_24h}) is determined from

$$E_{LS\_24h} = E_{PV\_24h} + E_{FC\_24h} + E_{GD\_24h}^{BUY} - E_{GD\_24h}^{SEL} + \Delta E_{BT\_24h} \quad (17)$$

where ΔE_{BT_24h} is the variation in the battery energy during the 24h time duration and is defined from

$$\Delta E_{BT\_24h} = E_{BT\_24h}^{DCH} - E_{BT\_24h}^{CHD} + E_{BT\_0h} - E_{BT\_24h} \quad (18)$$

where E_{BT_0h} and E_{BT_24h} are the stored energy in the battery at the beginning and the end of the 24h time interval, respectively, and are determined by the SOC level. On the other hand, to analyse the system operation economically, the total energy cost of each element x, ($C_{x\text{-}24h}$) is determined by the amount of the attributed power $P_x(k)$ and energy cost $C_x(k)$at the sampling time k from

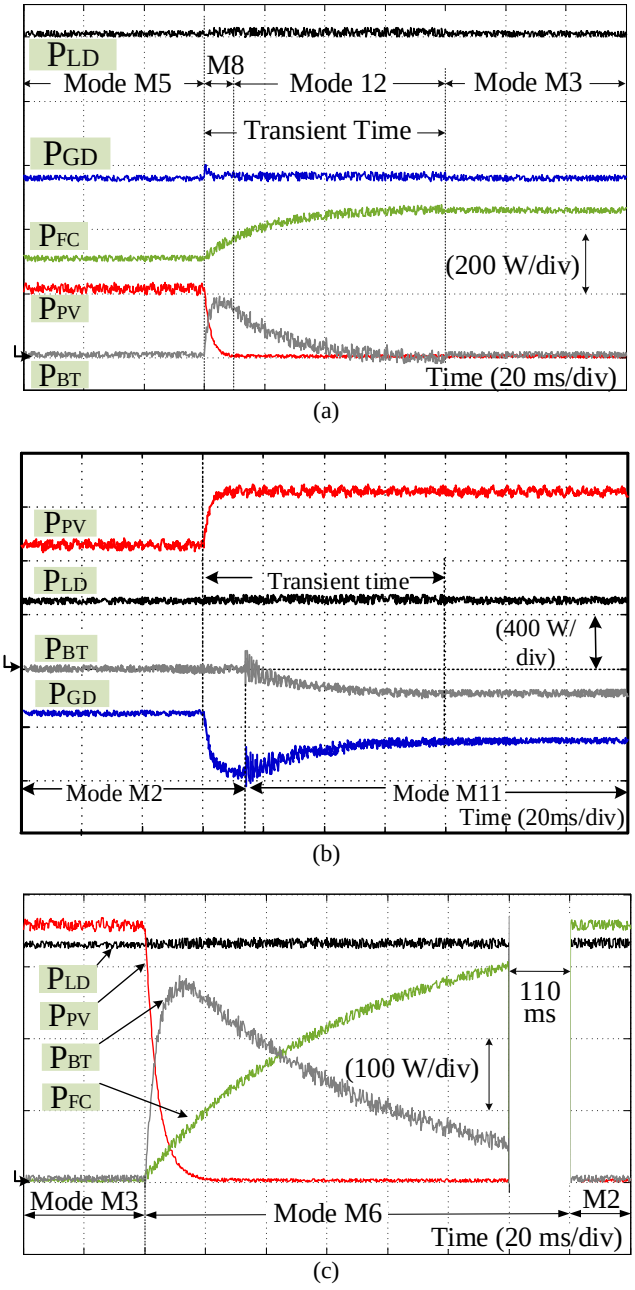

Fig.16. Experimentally measured powers of the micro-grid components during the mode transition process, (a) direct transition from M5 to M3 and, (b) transition from M2 to M11, (c) indirect mode transition from M3 to M2.

$$C_{x\_24h} = \sum_{k=1}^{720} P_{x\_24h}(k) C_{x\_24h}(k) T_k \quad (19)$$

The operation of the micro-grid elements and the EMU are analysed in more detail in the next sections. The objective function of the energy management is minimizing the consumer's bill from bidirectional energy transfer to the grid.

A. Energy Management in Grid-connected Condition

The EMU operation for two cases of PV power profiles in the sunny (the first scenario) and cloudy (the second scenario) weather conditions is experimentally tested. Fig.17 (a) presents the power profiles of the PV generation, load demand, fuel cell, battery, electrolyzer and the grid for the

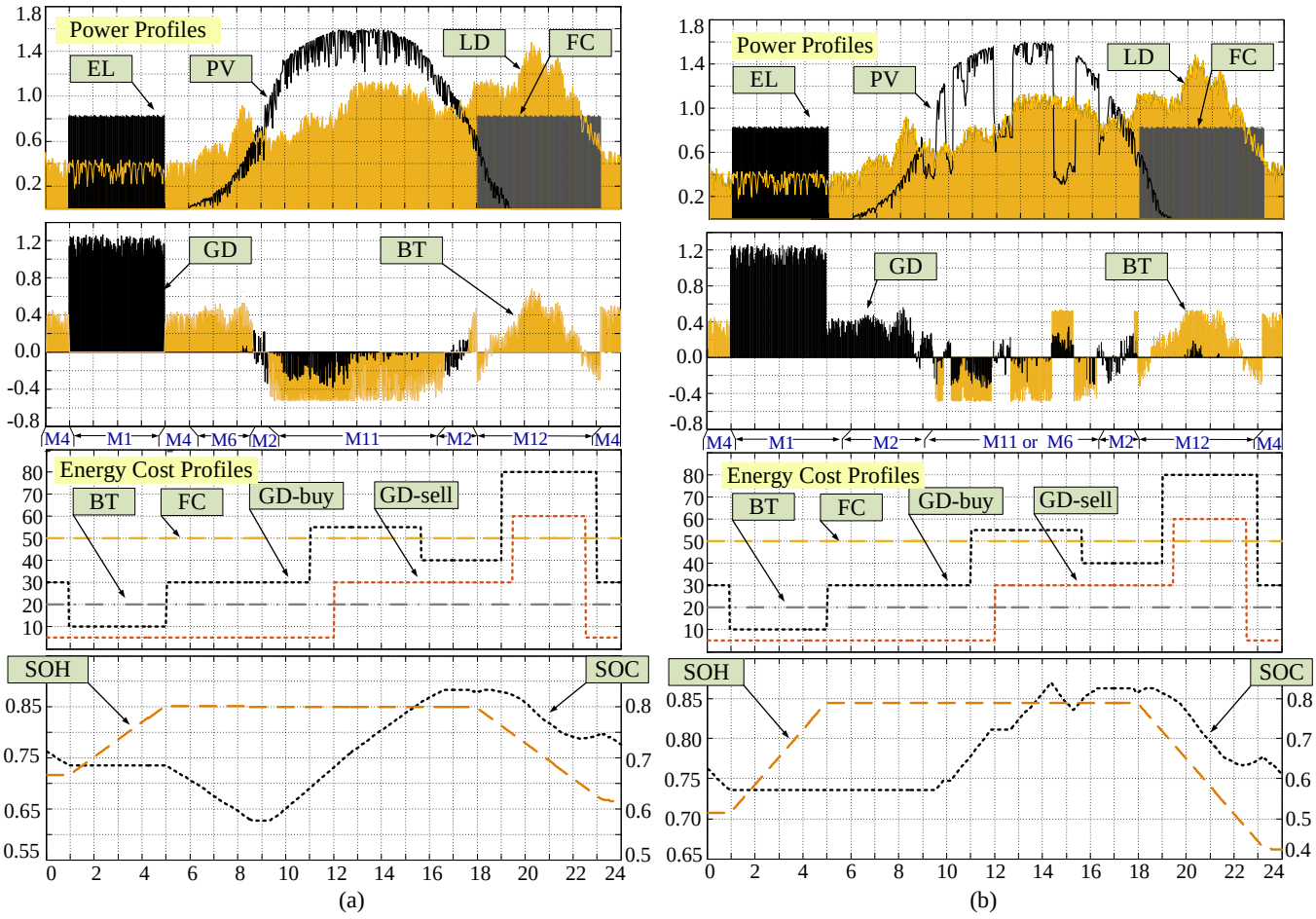

Fig.17. The experimentally recorded power profiles of the energy cost profiles, battery SOC and fuel cell SOH for (a) a sunny day and, (b) a cloudy day profiles

first scenario. The energy cost profiles of the fuel cell, battery and the grid and the estimated values of SOC and SOH are also presented. The energy cost of the PV and EL are assumed to be 0.02 and 0.01 $/kWh respectively considering their running and the capital cost.

The operation modes are presented at the bottom of the power profile. As can be seen, at the beginning M4 is selected where battery supplies the load due to the amount of load demand and lower energy cost compared to the grid. The mode then is changed to M1 when grid energy cost drops to less than the battery, the load is supplied by the grid and electrolyzer is activated. At 5 AM when grid energy cost increases to more than the battery, the operation mode changes back to M4. The PV generation starts at 6 AM and therefore the mode changes to M6 where the load is supplied by the PV and the battery. When the PV power is slightly less or more than the load demand, M2 is selected and the power is transferred to or received from the grid. Thanks to the predictive control, the battery is not selected due to the low-efficiency characteristics of the battery and converters in small powers. When the PV generation exceeds the load demand the operation mode changes to M11 where the surplus energy is preferred to charge the battery as it is predicted that the battery needs to supply the load in the peak demand hours. The additional energy is supplied to the grid due to the battery charging power limit. The PV generation is reduced close to the load demand, and M2 is selected again as already discussed. At peak demand hours, the load is preferred to be supplied mainly by the fuel cell and the battery considering the energy cost and M12 is selected as the operation mode. The energy received by the grid at this time is minimized as much as possible and the battery SOC and fuel cell SOH levels are almost maximized due to the successful operation of the long-term predictive control. Finally, at 11 PM when the load demand drops to less than the battery power, the operation mode is changed back to M4.

Fig.17 (b) presents the similar profiles of the power and energy cost for the second energy management scenario. The operation modes are presented in the figure and are selected based on the same principle. However, in the case of a cloudy profile, unlike the sunny day scenario, the battery is not discharged from 5 AM to 10 AM to supply the load. This is because it needs to preserve enough energy for the mid-day or peak demand hours due to the predicted poor PV generation. The successful operation of the predictive control in both scenarios results in a minimum difference between the battery SOC and the fuel cell SOH at the beginning and the end of the period which increases the management flexibility for the next day. Furthermore, the battery is not charged by the grid at the beginning of the period and it is delayed until the midday to be charged by the surplus energy of PV. As a result, the solar energy is used locally instead of being transferred to the grid, contributing more efficiently in the power shaving process. This can also reduce the consumer's energy bill by reducing the energy received from the grid at the peak energy cost period which is the main objective of the predictive control.

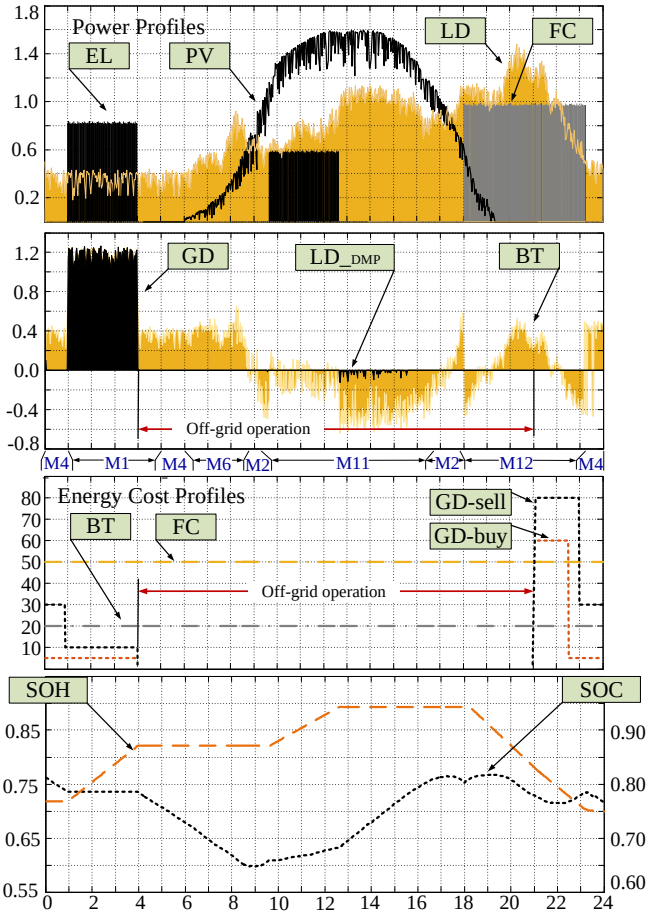

Fig.18. The experimentally recorded power profiles of the energy cost profiles, battery SOC and fuel cell SOH for a sunny day profile including an off-grid operation period from 4 AM to 9 PM.

B. Energy Management in Off-grid Condition

To demonstrate the operation of the proposed energy management technique in the off-grid condition, a third energy management scenario in which there is no access to the utility grid for a particular period due to the rolling blackout or a planned power outage is also presented. In this case, the objective function of the predictive control for long blackout periods can be changed to minimize the difference between the predicted load demand and supplied energy due to the grid absence. In this paper, it is assumed that the blackout period is scheduled and is already sent to the EMU by the RDNCC. However, in the case of an accidental power outage with an unknown period, the EMU operation is based on the real-time data of the system only. This case is not considered in this paper due to the complexity. Fig.18 illustrates the power and cost profiles of the micro-grid components with similar load demands, PV generation and cost profiles. As can be seen, the planned power outage period starts at 4 AM and ends at 9 PM. During this period the load is supplied only by the PV, battery and fuel cell. Compared to the previously discussed scenarios, the first electrolyzer activation mode is ended in a shorter time due to the start of the power outage period. Therefore, the surplus energy generated by the PV is supplied to the electrolyzer for another period to increase the SOH level due to the predicted operation of fuel cell in the peak demand hours. When the SOH level increases to the acceptable range, the surplus energy is then sent to the battery to increase the SOC level. In the case that the PV generation is more than the load demand plus the battery maximum

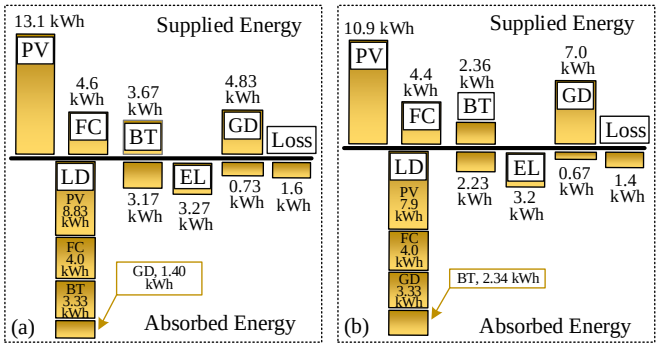

Fig.19. Energy distribution analysis (a) sunny and (b) cloudy day profiles

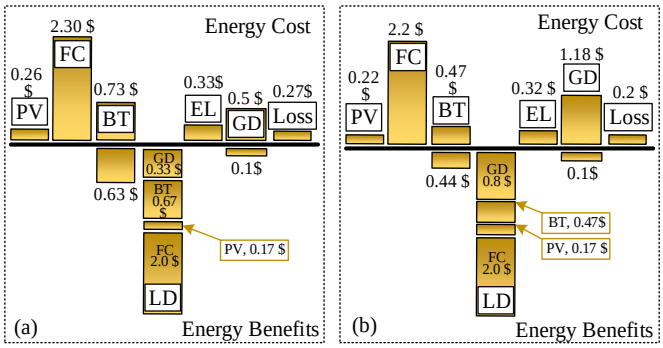

Fig.20. Energy cost analysis (a) sunny and (b) cloudy day profiles

charging power, the additional power is sent to a dump load (LD_DMP) due to the absence of the grid. The operation modes of the system in the off-grid condition are presented under the power profiles. As can be seen, there are two activation period for the electrolyzer due to the predictive control operation. Furthermore, the SOC and SOH levels at the beginning and the end of the test period are very close as a result of the predictive energy management.

The resultant value of energy attributed to each of the micro-grid elements is used to analyse the energy distribution of the system in the case of the first and second energy management scenarios as presented in Fig.19. As can be seen, almost 50 % of the load demand is covered by the PV in the sunny day profile. However, this reduced to 45 % in cloudy condition. The energy supplied to the load by the grid increased from 8 % to 19 % in the second case as the battery energy is saved for the peak demand hours due to the reduced PV power generation.

Fig.20 illustrates the daily energy cost analysis for the same scenarios and the period. As can be seen, the total energy cost for the sunny and cloudy days are 4.4 and 4.6 $/day respectively. However; this increases to 6 $/day in the case of using only grid energy with the same cost profile. About 50 % of the total energy cost belongs to the fuel cell compared to the other sources (≈2 $/day). The energy supplied to the grid is not considerable due to the limited amount of PV power generation. This can be achieved by increasing the PV panels and extracted power. The presented charts are extracted from the recorded data in the EMU using the graphical user interface (MATLAB/GUI).

V. Conclusion

A new energy management technique for a magnetically coupled micro-grid with 20 different grid-connected and off-grid operation modes is proposed in this paper. A predictive controller is designed to optimally manage the available

capacity of the storage devices according to the long-term energy plans, energy generation and consumption based on a dynamic programming method. The efficiency performance of the micro-grid components and the energy cost are included in the management process. On the other hand, a fuzzy controller is used to determine the operation mode of the system according to the real-time data. A mode transition strategy is designed to smooth the mode variation. A prototype of the proposed micro-grid and the energy management system are developed and experimentally tested for three different energy management scenarios. The effectiveness of the proposed energy management technique on reduction of consumer's electricity bill was approved.

REFERENCES

[1] Global Energy Transformation report 2018,a roadmap to 2050, https://www.irena.org/media/Files/IRENA/Agency/Publication/2018/Apr/IRENA_Report_GET_2018.pdf

[2] Solar report January2018, Australian Energy Council: https://www.energycouncil.com.au/media/11188/australian-energy-council-solar-report_-january-2018.pdf

[3] H. Gharavi and R. Ghafurian, "Smart grid: The electric energy system of the future," *Proc. IEEE*, vol. 99, no. 6, pp. 917–921, Jun. 2011.

[4] N. Hatziargyriou, "Microgrids: Architectures and Control," *Chichester*, U.K.:Wiley, pp. 1-24, 2014.

[5] N. Komninos, E. Philippou and A. Pitsillides, "Survey in Smart Grid and Smart Home Security: Issues, Challenges and Countermeasures," *IEEE Communications Surveys & Tutorials*, vol. 16, no. 4, pp. 1933-1954, Fourthquarter 2014.

[6] T. Li and M. Dong, "Residential Energy Storage Management with Bidirectional Energy Control," *IEEE Trans. Smart Grid*.

[7] L. Igualada, C. Corchero, M. Cruz-Zambrano and F. J. Heredia, "Optimal Energy Management for a Residential Microgrid Including a Vehicle-to-Grid System," *IEEE Tran. Smart Grid*, vol. 5, no. 4, pp. 2163-2172, July 2014.

[8] D. Livengood and R. Larson, "The energy box: Locally automated optimal control of residential electricity usage," *Service Science*, vol.1, no. 1, pp. 1–16, 2009.

[9] http://www.cleanenergyregulator.gov.au/RET/Scheme-participants-and-industry/Agents-and-installers/Installation-requirements-for-small-scale-systems

[10] M. Erol-Kantarci and H. T. Mouftah, "Wireless sensor networks for cost-efficient residential energy management in the smart grid," *IEEE Trans. Smart Grid*, vol. 2, no. 2, pp. 314_325, Jun. 2011.

[11] H. Ghazzai and A. Kadri, "Joint Demand-Side Management in Smart Grid for Green Collaborative Mobile Operators Under Dynamic Pricing and Fairness Setup," *IEEE Trans. Green Communications and Networking*, vol. 1, no. 1, pp. 74-88, March 2017.

[12] BS.Hartono, S.P.Mursid and S.PrajogoReview, "Home energy management system in a Smart Grid scheme to improve reliability of power systems," *Earth and Environmental Science*, Vol.105, conference 1,10.1088/1755-1315/105/1/012081

[13] N. Javaid, I. Khan, M. N. Ullah, A. Mahmood and M. U. Farooq, "A Survey of Home Energy Management Systems in Future Smart Grid Communications," *in proc. Eighth Int. Con on Broadband and Wireless Computing, Communication and Applications, Compiegne*, 2013, pp. 459-464

[14] N. Komninos, E. Philippou and A. Pitsillides, "Survey in Smart Grid and Smart Home Security: Issues, Challenges and Countermeasures," *IEEE Communications Surveys & Tutorials*, vol. 16, no. 4, pp. 1933-1954, Fourthquarter 2014.

[15] D. Arcos-Aviles, J. Pascual, L. Marroyo, P. Sanchis, F. Guinjoan, "Fuzzy Logic-Based Energy Management System Design for Residential Grid-Connected Microgrids," *IEEE Trans. Smart Grid* , vol. PP, no.99, pp.1-1

[16] L. Igualada, C. Corchero, M. Cruz-Zambrano and F. J. Heredia, "Optimal Energy Management for a Residential Microgrid Including a Vehicle-to-Grid System,"*IEEE Trans. Smart Grid*, vol. 5, no. 4, pp. 2163-2172, July 2014.

[17] Z. Zhao, P. Yang, J. M. Guerrero, Z. Xu and T. C. Green, "Multiple-Time-Scales Hierarchical Frequency Stability Control Strategy of Medium-Voltage Isolated Microgrid," *IEEE Trans. Power Elec*, vol. 31, no. 8, pp. 5974-5991, Aug. 2016.

[18] M. Jafari, Z. Malekjamshidi, G. Lei, T. Wang, G. Platt and J. Zhu, "Design and Implementation of an Amorphous High-Frequency Transformer Coupling Multiple Converters in a Smart Microgrid," *IEEE Trans. Ind. Elec*, vol. 64, no. 2, pp. 1028-1037, Feb. 2017.

[19] M. Jafari, Z. Malekjamshidi and J. Zhu, "Copper Loss Analysis of a Multi-winding High-frequency Transformer for a Magnetically-coupled Residential Micro-grid," *IEEE Trans. Ind. Applications*. doi: 10.1109/TIA.2018.2864170

[20] H. Tao, A. Kotsopoulos, J. L. Duarte and M. A. M. Hendrix, "Transformer-Coupled Multiport ZVS Bidirectional DC–DC Converter With Wide Input Range," *IEEE Trans. Power Elec.*, vol. 23, no. 2, pp. 771-781, March 2008.

[21] C. Zhao, S. D. Round and J. W. Kolar, "An Isolated Three-Port Bidirectional DC-DC Converter With Decoupled Power Flow Management," *IEEE Trans. Power Elec.*, vol. 23, no. 5, pp. 2443-2453, Sept. 2008.

[22] H. Yin, W. Zhou, M. Li, C. Ma and C. Zhao, "An Adaptive Fuzzy Logic-Based Energy Management Strategy on Battery/Ultracapacitor Hybrid Electric Vehicles," *IEEE Trans. Transportation Electrification*, vol. 2, no. 3, pp. 300-311, Sept. 2016.

[23] H. Fakham, D. Lu and B. Francois, "Power Control Design of a Battery Charger in a Hybrid Active PV Generator for Load-Following Applications," *IEEE Trans. Ind. Elec*, vol. 58, no. 1, pp. 85-94, Jan. 2011.

[24] P. García, J. P. Torreglosa, L. M. Fernández, F. Jurado, "Optimal energy management system for stand-alone wind turbine/ photovoltaic/hydrogen/battery hybrid system with supervisory control based on fuzzy logic," *Int. J. Hydrogen Energy*, vol. 38, no. 33, pp. 14146-14158, Nov. 2013.

[25] Hao Ying, "Basic Fuzzy Mathematics for Fuzzy Control and Modeling," *Fuzzy Control and Modeling:Analytical Foundations and Applications* , 1, Wiley-IEEE Press, 2000, pp.342-

[26] A. A. Ferreira, J. A. Pomilio, G. Spiazzi and L. de Araujo Silva, "Energy Management Fuzzy Logic Supervisory for Electric Vehicle Power Supplies System," *IEEE Trans. Power Elec.*, vol. 23, no. 1, pp. 107-115, Jan. 2008.

[27] R. Zhang, J. Tao and H. Zhou, "Fuzzy optimal energy management for fuel cell and supercapacitor systems using neural network based driving pattern recognition," *IEEE Trans. Fuzzy Systems*. doi: 10.1109/TFUZZ.2018.2856086

[28] Lagorse.J, Simoes.M.G, Miraoui.A, "A multiagent fuzzy-logic-based energy management of hybrid systems," *IEEE Trans. Ind. Appl.*, vol. 45, no. 6, pp. 2123-2129, Nov.-Dec. 2009

[29] D. Shahgoshtasbi and M. M. Jamshidi, "A New Intelligent Neuro–Fuzzy Paradigm for Energy-Efficient Homes," *IEEE Systems Journal*, vol. 8, no. 2, pp. 664-673, June 2014.

[30] Z. Wu, X. Zhang, J. Brandt, S. Zhou and J. LI, "Three Control Approaches for Optimized Energy Flow With Home Energy Management System," *IEEE Power and Energy Technology Systems Journal*, vol. 2, no. 1, pp. 21-31, March 2015.

[31] M. Jafari, Z. Malekjamshidi, D. D. C. Lu and J. Zhu, "Development of a Fuzzy-Logic-Based Energy Management System for a Multi-Port Multi-Operation Mode Residential Smart Micro-grid," *IEEE Trans. Power Elec.* doi: 10.1109/TPEL.2018.2850852

[32] Aishwarya Panday and H. O. Bansal, "Energy management strategy for hybrid electric vehicles using genetic algorithm," *J. Renew. Sustain. Energ.*, vol. 8, no. 1, pp. 741-746, Jan. 2016.

[33] Y. Ates, O. Erdinc, M. Uzunoglu, and B. Vural, "Energy management of an FC/UC hybrid vehicular power system using a combined neural network-wavelet transform based strategy*," Int. J. Hydrogen Energy*., vol. 35, no. 2, pp. 774-783, Jan. 2010.

[34] M. K. Dayeni and M. Soleymani, "Intelligent energy management of a fuel cell vehicle based on traffic condition recognition," *Clean Technol. Environ. Policy*, vol. 18, no. 6, pp. 1945–1960, Aug. 2016.

[35] D. Fares, R. Chedid, F. Panik, S. Karaki, and R. Jabr, "Dynamic programming technique for optimizing fuel cell hybrid vehicles," *Int. J. Hydrogen Energy*., vol. 40, no. 24, pp. 7777-7790, Jun. 2015.

[36] M.Jafari, Z.Malekjamshidi, and J.Zhu, "A magnetically coupled multi-port, multi-operation-mode micro-grid with a predictive dynamic programming-based energy management for residential applications," *International Journal of Electrical Power & Energy Systems*, vol. 104, no. January 2019, pp. 784-796

[37] Y. Riffonneau, S. Bacha, F. Barruel and S. Ploix, "Optimal Power Flow Management for Grid Connected PV Systems With Batteries," *IEEE Trans.Sustainable Energy*, vol. 2, no. 3, pp. 309-320, July 2011.

[38] T. T. H. Pham, F. Wurtz and S. Bacha, "Optimal operation of a PV based multi-source system and energy management for household application," *2009 IEEE International Conference on Industrial Technology*, Gippsland, VIC, 2009, pp. 1-5.

[39] A. Borghetti, C. D'Ambrosio, A. Lodi and S. Martello, "An MILP Approach for Short-Term Hydro Scheduling and Unit Commitment With Head-Dependent Reservoir," *IEEE Trans. Power Systems*, vol. 23, no. 3, pp. 1115-1124, Aug. 2008.
[40] Bo Lu and M. Shahidehpour, "Short-term scheduling of battery in a grid-connected PV/battery system," *IEEE Trans. Power Systems*, vol. 20, no. 2, pp. 1053-1061, May 2005.
[41] R. Palma-Behnke, C. Benavides, F. Lanas, B. Severino, L. Reyes, J. Llanos, and D. Saez, "A microgrid energy management system based on the rolling horizon strategy," *IEEE Trans. Smart Grid*, vol. 4, no. 2, pp. 996–1006, Jun. 2013.
[42] Q. Jiang, M. Xue, and G. Geng, "Energy management of microgrid in grid-connected and stand-alone modes," *IEEE Trans. Power Syst.*, vol. 28, no. 3, pp. 3380–3389, Aug. 2013.
[43] R. Miceli, "Energy Management and Smart Grids," Energies 2013, 6, 2262-2290.
[44] E. Muljadi and H. Ed. McKenna, "Power quality issues in a hybrid power system," *IEEE Trans. Ind. Appl.*, vol. 38, no. 3, pp. 803–809, May/Jun. 2002.
[45] Y. Zhang, A. A. Chowdhury, and D. O. Koval, "Probabilistic wind energy modeling in electric generation system reliability assessment," *IEEE Trans. Ind. Appl.*, vol. 47, no. 3, pp. 1507–1514, May/Jun. 2011.
[46] P. Fortenbacher, J. L. Mathieu and G. Andersson, "Modeling and Optimal Operation of Distributed Battery Storage in Low Voltage Grids," *IEEE Trans. Power Systems*, vol. 32, no. 6, pp. 4340-4350, Nov. 2017.

Mohammad Jafari (M'12) received the B.E. degree from Shiraz University, Shiraz, Iran, in 1998, the M.E. degree from Guilan University, Rasht, Iran, in 2001 and, the Ph.D. degree from University of Technology Sydney (UTS), Sydney, Australia, in 2017 all in electrical engineering. From 2001 to 2011, he contributed to the design and development of industrial power electronic projects. Since 2012, he has been with the UTS as a lecturer. His current research interests include power electronic converters and drives, renewable energy systems and smart micro-grids.

Zahra Malekjamshidi (S'13) received the B.E. and M.E. degrees from Shiraz University, Shiraz, Iran, in 1998, and 2001 respectively, both in electrical engineering. She is currently working toward the Ph.D. degree at the University of Technology Sydney (UTS), Sydney, Australia. From 2002 to 2012, she worked as a research engineer and contributed to the design and development power electronic projects. Her current research interests include matrixconverters, dc-dc converters, renewable energy technologies and smart micro-grids.

Jianguo Zhu (S'93–M'96–SM'03) received the B.E. degree in 1982 from Jiangsu Institute of Technology, Jiangsu, China, the M.E. degree in 1987 from Shanghai University of Technology, Shanghai, China, and the Ph.D. degree in 1995 from the University of Technology Sydney (UTS), Sydney, Australia, all in electrical engineering. He was appointed a lecturer at UTS in 1994 and promoted to full professor in 2004 and Distinguished Professor of Electrical Engineering in 2017. In 2018, he joined the University of Sydney, Australia, as a full professor and Head of School, School of Electrical and Information Engineering. His research interests include computational electromagnetics, measurement and modelling of magnetic properties of materials, electrical machines and drives, power electronics, renewable energy systems and smart micro grids.

Mohammad-Hassan Khooban (M'13-SM'18) was born in Shiraz, Iran, in 1988. He received the Ph.D. degree from Shiraz University of Technology, Shiraz, Iran, in 2017. He was a research assistant with the University of Aalborg, Aalborg, Denmark from 2016 to 2017 conducting research on Microgrids and Marine Power Systems. Currently, he is a PostDoctoral Associate at Aalborg University, Denmark. His research interests include control theory and application, power electronics and its applications in power systems, industrial electronics, and renewable energy systems. He is author or co-author of more than 100 publications on journals and international conferences, plus one book chapter and one patent. He is currently serving as an Associate Editor of the Complexity Journal.